Interpreting attenuation at different excitation amplitudes to estimate strain-dependent interfacial rheological properties of lipid-coated monodisperse microbubbles

Lang Xia,[1] Tyrone M. Porter,[2] and Kausik Sarkar[1,a)]
[1]*Department of Mechanical and Aerospace Engineering, The George Washington University, Washington, DC 20052, USA*
[2]*Department of Mechanical Engineering, Boston University, Boston, Massachusetts 02215, USA*

(Received 4 September 2015; revised 5 December 2015; accepted 7 December 2015; published online 30 December 2015)

Broadband attenuation of ultrasound measured at different excitation pressures being different raises a serious theoretical concern, because the underlying assumption of linear and independent propagation of different frequency components nominally requires attenuation to be independent of excitation. Here, this issue is investigated by examining ultrasound attenuation through a monodisperse lipid-coated microbubble suspension measured at four different acoustic excitation amplitudes. The attenuation data are used to determine interfacial rheological properties (surface tension, surface dilatational elasticity, and surface dilatational viscosity) of the encapsulation according to three different models. Although different models result in similar rheological properties, attenuation measured at different excitation levels (4–110 kPa) leads to different values for them; the dilatation elasticity (0.56 to 0.18 N/m) and viscosity (2.4×10^{-8} to 1.52×10^{-8} Ns/m) both decrease with increasing pressure. Numerically simulating the scattered response, nonlinear energy transfer between frequencies are shown to be negligible, thereby demonstrating the linearity in propagation and validating the attenuation analysis. There is a second concern to the characterization arising from shell properties being dependent on excitation amplitude, which is not a proper constitutive variable. It is resolved by arriving at a strain-dependent rheology for the encapsulation. The limitations of the underlying analysis are discussed. © *2015 Acoustical Society of America*.
[http://dx.doi.org/10.1121/1.4938234]

[CCC] Pages: 3994–4003

I. INTRODUCTION

Microbubbles (diameter $< 10\,\mu$m) are excellent agents for increasing the contrast-to-tissue ratio of medical ultrasound images (Goldberg *et al.*, 2001). They are stabilized against premature dissolution via gas diffusion by a monolayer of proteins, lipids, or other surface active molecules (Katiyar *et al.*, 2009; Sarkar *et al.*, 2009; Katiyar and Sarkar, 2010). The monolayer encapsulation also critically affects the scattering properties of the contrast microbubbles (deJong *et al.*, 1991; deJong, 1996). Many mechanical models have been developed to describe this effect (deJong *et al.*, 1992; Church, 1995; Hoff *et al.*, 2000; Morgan *et al.*, 2000; Chatterjee and Sarkar, 2003; Marmottant *et al.*, 2005; Sarkar *et al.*, 2005; Doinikov and Dayton, 2007; Paul *et al.*, 2010). They have been applied to experimental measurements to estimate mechanical properties of various contrast microbubbles. However, contrast agents are usually polydisperse making accurate shell property estimation using bulk experimental measurement difficult. In this article, we estimate the shell properties of a lipid-coated monodisperse microbubble applying several different mathematical models to ultrasound attenuation measured at different excitation amplitudes. However, the more important objectives of this paper are validation of the analysis. Here we investigate the validity of the excitation amplitude-dependent attenuation data and reconcile it with the principle of linearity that underlie frequency-dependent attenuation. We also relate the shell properties dependent on excitation amplitude—the latter not being a constitutive variable—to dependent on material strain.

Due to the polydispersity of a contrast agent suspension, acoustic experiments—attenuation and scattering—access bulk dynamics resulting from the integrated effects of the entire size distribution (deJong *et al.*, 1992; Chatterjee and Sarkar, 2003; Chatterjee *et al.*, 2005a; Paul *et al.*, 2012). The size distribution of a contrast agent typically ranging from submicron to tens of micron is notoriously difficult to determine. On the other hand, high frame-rate optical observations, although they determine accurate single bubble radial dynamics, are typically performed on a microbubble from the larger size end of the entire size distribution (Morgan *et al.*, 2000; Patel *et al.*, 2002; Marmottant *et al.*, 2005). Recently, one of the coauthors (T.P.) adopted a method to synthesize monodisperse lipid-coated microbubbles using a flow focusing microfluidic device (Gong *et al.*, 2010). In a recently published letter, henceforth referred to as GCP, his group measured ultrasound attenuation through such a monodisperse suspension to find that the attenuation spectrum has a sharp peak, which shifts to lower values with increasing excitation amplitude (Gong *et al.*, 2014). Note

a)Electronic mail: sarkar@gwu.edu

that at resonance, the acoustic activity of a microbubble is considerably higher than off resonance, resulting in orders of magnitude higher values for scattering and attenuation cross sections (Medwin, 1977; Sarkar and Prosperetti, 1994). Therefore, the peak of the attenuation spectrum occurs at the bubble resonance frequency and its downshift with excitation pressure can be interpreted as a reduction in the "spring constant" of the system. From the linearized equations of encapsulated microbubble dynamics, one can relate it to pressure-dependent mechanical properties—with increasing pressure, as the bubble experiences larger oscillations, the shell elasticity decreases. Gong *et al.* (2014) accordingly obtained decreasing shell elasticity as a function of increasing acoustic pressure amplitude in GCP. Here, we extend the analysis to the determination of the complete interfacial rheology, viz., surface dilatational elasticity as well as damping constant represented by surface dilatational viscosity. We also subject the analysis to a critical scrutiny examining the underlying assumption and the validity of the attenuation analysis.

There are two concerns that can be justifiably raised against the above analysis of the attenuation data. The first one relates to the linearity underlying the theory of acoustic attenuation. The computation of attenuation cross-sections or attenuation coefficients presupposes the acoustic wave propagation to be linear, where each frequency component present in an acoustic pulse propagates independently of the others. This assumption allows one to compute the damping of each component from the linear Fourier analysis by computing FFT of the received pulse and comparing it with the incident pulse. Linearity demands therefore that the analytical expression of the attenuation coefficient should not depend on the pulse pressure amplitude, as was investigated by us previously (Chatterjee *et al.*, 2005b), in contrast to the observation mentioned above. The second concern stems from the lack of a rational basis for direct dependence of shell properties on the amplitude of ultrasound pulse. As stated above, this relation results from larger oscillations at higher excitations signifying a dependence on the strain or the change in area fraction rather than the amplitude of the pressure pulse. Both of these issues have been investigated here. Specifically, we investigate whether nonlinearity in bubble dynamics, indicated by different behaviors at different excitations, invalidates the analysis of the data using the linear theory of acoustic attenuation. Furthermore, we relate shell properties to strain, i.e., we establish an approximate "strain-softening shell" model for describing the pressure-dependent shell properties.

Note that we have previously incorporated "strain-softening" in the interfacial rheological model of a microbubble encapsulation by a nonlinear exponentially varying surface elasticity model EEM (Paul *et al.*, 2010). As mentioned above, there have been numerous models of contrast agent encapsulation starting with early work by de Jong *et al.* (deJong *et al.*, 1992) and the first rigorous thick-shell model of Church (Church, 1995; Hoff *et al.*, 2000). In view of the typically monolayer nature of the shell, in 2003, we proposed a zero-thickness interfacial rheological model of the encapsulation assuming a purely Newtonian rheology (Newtonian model NM) (includes surface tension and surface dilatational viscosity) (Chatterjee and Sarkar, 2003). It was subsequently modified to include a surface dilatational elasticity—constant elasticity model (CEM) (Sarkar *et al.*, 2005)—and later a strain-softening nonlinear surface elasticity model (EEM) (Paul *et al.*, 2010). Marmottant *et al.* proposed an elegant model (MM) which is identical to CEM but includes two additional parameters that represents important physics of shell buckling and rupture (Marmottant *et al.*, 2005).

Here, we measure attenuation through a monodisperse lipid-coated microbubble suspension at different excitation amplitudes and apply three different models—NM, CEM, and MM—to characterize them finding the interfacial rheological parameters. In Sec. II, the methods and mathematical formulations are provided. Section III discusses the results investigating the validity of the analysis and proper interpretation of the result. The findings are summarized in the final section.

II. METHODS

A. Monodisperse microbubble preparation

A flow-focusing microfluidic device has been designed to create monodisperse lipid-coated microbubbles. The procedure has been described in detail previously (Gong *et al.*, 2010), and therefore will only be described briefly here. Bubbles were generated by forcing co-flowing streams of gas and liquid through a small 7 μm orifice. The width of the size distribution was kept narrow by a constant flow rate and gas pressure controlled by a syringe pump (KDS100, Fisher Scientific); their values determine the mean microbubble size. The microbubbles were made from a lipid solution—a mixture of DSPC (1,2-distearoyl-sn-glycero-3-phosphocholine) and DSPE-PEG2000 (1,2-distearoyl-sn-glycero-3-phosphoethanolamine-N-[Methoxy (polyethylene glycol)–2000]) combined at a molar ratio of 9:1 and octafluoropropane. The lipids were bought from Avanti Polar Lipids Inc. (Alabaster, AL). The mixture was dissolved in chloroform ($CHCl_3$) to get a uniform solution, dried under argon, and the resultant film was further dried under vacuum to ensure complete removal of the organic solvent. The lipid film was rehydrated with saline solution, sonicated for 20 min in an ice bath, and the resultant vesicles were suspended in a solution of 10% glycerol, 10% propylene glycol, and 80% deionized water. By using a sparging system, the lipid solution is air degassed at room temperature overnight. Then octafluoropropane was introduced into the flask via a three-way stopcock to reach atmosphere pressure, and circulated overnight by a pump dive (Masterflex console drive, Cole-Parmer). The size distribution (Fig. 1) shows largely a monodisperse population with a mean diameter of 5.2 μm. For the attenuation experiments, there were about 25 000 microbubbles/ml (measured with a Coulter counter) injected into a sample chamber.

B. Attenuation measurement

Figure 2 shows the experimental setup for measuring sound attenuation. Two matched single-element unfocused transducers (Panametrics, with 2.25 MHz center frequency and 1/2′ aperture diameter) were used as transmitter and receiver to measure broadband attenuation in a through-transmission

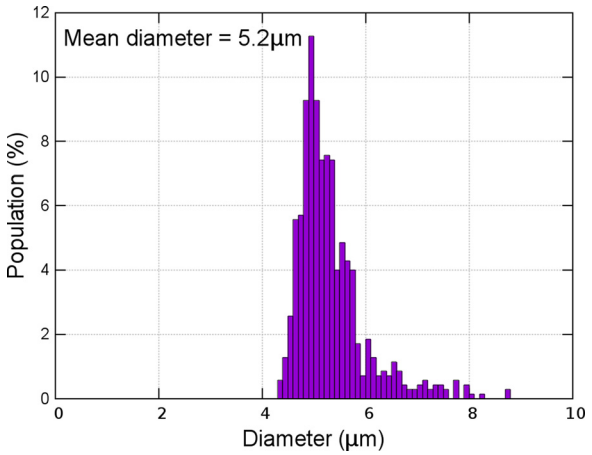

FIG. 1. (Color online) Size distribution of the monodisperse lipid-coated microbubbles.

configuration. The microbubble suspension was injected into an exposure chamber, which consisted of a latex sheet pulled over a plastic frame. The exposure chamber with a thickness $d = 1.3$ cm was submerged in a tank of degassed deionized water in front of a stainless steel (SS) plate, which served as a perfect reflector. The broadband pulse, driven by a pulser/receiver (5072PR, Panametrics) with a pulse repetition frequency (PRF) of 100 Hz traveled a distance of $L = 9$ cm before reaching the receiving transducer. The received pulse was amplified by the pulser/receiver and digitized (fs = 2.5 GHz/s) with a digital oscilloscope (Wavesurfer 64XS, LeCroy) before being saved on a desktop computer for frequency analysis. All received signals were processed using Matlab software (The Math Works, Inc., Natick, MA). The broadband attenuation was measured at four different peak negative pressures 4, 16, 40, and 110 kPa. The transducers were calibrated using a 0.2 mm needle hydrophone (Precision Acoustics Dorset, UK). The experiment was completed in minutes with minimum gas diffusion and lipid dissolution. At each excitation level, 100 data sets have been acquired and averaged.

C. Mathematical models of encapsulation and bubble dynamics

The dynamics of an encapsulated microbubble is governed by a Rayleigh-Plesset (RP) type equation. The four different models—NM, CEM, EEM, and MM—have all been described in detail in their original publications (Chatterjee and Sarkar, 2003; Marmottant *et al.*, 2005; Sarkar *et al.*, 2005; Paul *et al.*, 2010) as well as our subsequent publication (Paul *et al.*, 2012). However, for the sake of completeness, we briefly describe them here. We have shown that all models—including those that represent the shell as having a finite thickness and consisting of materials with bulk material properties—can be expressed in a single interfacial framework with the following Rayleigh-Plesset (RP) equation (Katiyar and Sarkar, 2011):

$$\rho\left(R\ddot{R}+\frac{3}{2}\dot{R}^2\right)=P_{G_0}\left(\frac{R_0}{R}\right)^{3\kappa}\left(1-\frac{3\kappa\dot{R}}{c}\right)-\frac{2}{R}\gamma(R)-\frac{4\dot{R}}{R^2}\kappa^s(R)-4\mu\frac{\dot{R}}{R}-p_0+p_A(t). \tag{1}$$

The encapsulation is characterized by an effective surface tension $\gamma(R)$ and a dilatational viscosity $\kappa^s(R)$. R is the time-dependent bubble radius, $\dot{R}$ and $\ddot{R}$ are the first and the second-order time derivatives of the bubble radius, c is the velocity of sound in the surrounding liquid, $\rho = 1000\,\text{kg/m}^3$ is the liquid density, $\mu = 0.001$ Ns/m^2 is the liquid viscosity, R_0 is the initial bubble radius, P_{G_0} is the initial inside gas pressure, p_0 is the ambient pressure, and $p_A(t)$ is the excitation pressure. Gas diffusion is neglected. The inside gas pressure obeys a polytropic law with index κ. Since with oscillations at MHz frequency Peclet number $Pe = R_0^2\omega/D_g \gg 1$ (D_g is the thermal diffusivity, 2.8×10^{-6} m^2/s for C_3F_8), we assume an adiabatic behavior for the gas inside ($\kappa = 1.07$ for C_3F_8). The four different models for the encapsulation along with the resonance frequency $f_0 = \omega_0/2\pi$ of the corresponding dynamics predicted by the linearized form of Eq. (1) are given below.

Newtonian model (NM) (Chatterjee and Sarkar, 2003):

$$\gamma(R) = \gamma\,(\text{constant}) \text{ and } \kappa^s(R) = \kappa^s\,(\text{constant}), \tag{2}$$

$$f_0 = \frac{1}{2\pi R_0}\sqrt{\frac{1}{\rho}\left(3\kappa p_0+\frac{2\gamma}{R_0}(3\kappa-1)\right)}. \tag{3}$$

Constant elasticity viscoelastic model (CEM) (Chatterjee et al., 2005a):

$$\gamma(R) = \gamma_0 + E^s\beta,$$
$$\beta = \left(\frac{\Delta\text{Area}}{\text{Area}_{\text{equilibrium}}}\right) = \left(\frac{R^2}{R_E^2}-1\right) \quad \text{and}$$
$$\kappa^s(R) = \kappa^s(\text{constant}), \tag{4}$$

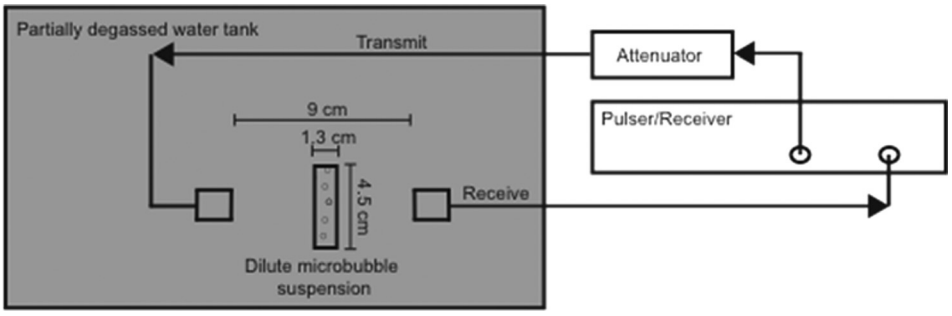

FIG. 2. Schematic of the setup for measuring frequency-dependent attenuation coefficient.

where γ_0 is a constant, a reference value of the interfacial tension and E^s is the constant dilatational elasticity. The equilibrium radius R_E is given by $R_E = R_0(1-\gamma_0/E^s)^{-1/2}$. This ensures a balance of inside and outside pressure at initial radius. At the equilibrium radius the bubble encapsulation has no elastic stresses

$$f_0 = \frac{1}{2\pi R_0}\sqrt{\frac{1}{\rho}\left(3\kappa p_0 - \frac{4\gamma_0}{R_0} + \frac{4E^s}{R_0}\right)}. \tag{5}$$

Viscoelastic model with exponentially varying elasticity (EEM) (Paul et al., 2010):

Even though, we do not explicitly use this model here, we later use the idea embedded in this model to arrive at a proper interpretation of the pressure-dependent rheology

$$\begin{aligned}\gamma(R) &= \gamma_0 + E^s\beta \\ E^s &= E_0^s\exp(-\alpha^s\beta)\end{aligned} \quad \text{and } \kappa^s(R) = \kappa^s \text{ (constant)}. \tag{6}$$

Enforcing the balance of pressure at initial radius we have an expression of equilibrium radius given by

$$R_E = R_0\left[1 + \left(\frac{1-\sqrt{1+4\gamma_0\alpha^s/E_0^s}}{2\alpha}\right)\right]^{-1/2}, \tag{7}$$

$$f_0 = \frac{1}{2\pi R_0}\sqrt{\frac{1}{\rho}\left(3\kappa p_0 + \frac{2E_0^s}{R_0}\left(\frac{\sqrt{1+4\gamma_0\alpha^s/E_0^s}}{\alpha^s}\right)\left(1+2\alpha^s - \sqrt{1+4\gamma_0\alpha^s/E_0^s}\right)\right)}. \tag{8}$$

Marmottant model (MM) (Marmottant et al., 2005):

$$\gamma(R) = \begin{cases} 0 & \text{for } R \le R_{\text{buckling}} \\ \chi\left(\dfrac{R^2}{R_{\text{buckling}}^2} - 1\right) & \text{for } R_{\text{buckling}} \le R \le R_{\text{rupture}} \text{ and } \kappa^s(R) = \kappa^s \text{ (constant)} \\ \gamma_w & \text{for } R \ge R_{\text{rupture}}, \end{cases} \tag{9}$$

where χ [same as E^s in Eq. (4)] is the elastic modulus of the shell, $R_{\text{buckling}} = R_0[1+\gamma(R_0)/\chi]^{-1/2}$, and $R_{\text{rupture}} = R_{\text{buckling}}[1+\gamma_w/\chi]^{1/2}$. Above R_{rupture}, the bubble is assumed to have a pure air-water interface and below R_{buckling}, it is in a buckled state where the effective interfacial tension is zero

$$f_0 = \frac{1}{2\pi R_0}\sqrt{\frac{1}{\rho}\left(3\kappa p_0 + \frac{2\gamma(R_0)}{R_0}(3\kappa-1) + \frac{4\chi}{R_0}\right)}. \tag{10}$$

D. Theory of acoustic attenuation

The extinction or attenuation cross section σ_e (Sarkar *et al.*, 1994; Medwin, 1977) is given by the relation

$$\sigma_e = 4\pi R_0^2\frac{c\delta}{\omega_0 R_0}\frac{\Omega^2}{\left[(1-\Omega^2)^2 + \Omega^2\delta^2\right]}, \qquad \Omega = \frac{\omega_0}{\omega} = \frac{f_0}{f}, \tag{11}$$

where $\omega = 2\pi f$ is the circular frequency. δ is the total damping that has three different contributions due to liquid viscosity, shell viscosity and acoustic reradiation (Sarkar *et al.*, 2005)

$$\begin{aligned}\delta &= \delta_{\text{liquid}} + \delta_{\text{encapsulation}} + \delta_{\text{radiation}} \\ &= \frac{4\mu}{\rho\omega_0 R_0^2} + \frac{4\kappa^s}{\rho\omega_0 R_0^3} + \frac{3\kappa P_0}{\rho\omega_0 R_0 c}.\end{aligned} \tag{12}$$

The encapsulation damping is by far the largest component of the three for contrast microbubbles (Katiyar and Sarkar, 2012). The thermal damping is neglected. Note that thermal and radiation damping have been investigated in detail in the literature and most recently a careful review (Ainslie and Leighton, 2011) shows the relative contributions and the analytical result justifies ignoring their contributions. Furthermore, we checked that accounting for thermal damping did not change the results of this paper. The frequency-dependent attenuation coefficients $\alpha(\omega)$ in dB/distance is

$$\begin{aligned}\alpha(\omega) &= 10\log_{10}e\int_{R_{\min}}^{R_{\max}}\sigma_e(a;\omega)n(a)da \\ &= 10(\log_{10}e)n\sigma_e,\end{aligned} \tag{13}$$

where e is the base of natural logarithm, $n(a)da$ is the number of bubbles per unit volume with radii in the range $(a, a+da)$, and the range of bubble radii is given by ($R_{\min}$, $R_{\max}$). The last part of the above equation arises due to the monodisperse nature of the contrast agent under consideration with $n = 2.5\times10^{10}$ microbubbles/m^3. The bubble separation is more than 100 times its radius indicating negligible bubble–bubble interactions. A careful investigation of sound propagation through bubbly liquid using multiple scattering theory of Foldy identified attenuation with the incoherent part of the average pressure wave (Sarkar and Prosperetti, 1994).

However, note that the above analysis assumes *linear* acoustic wave propagation, where the broadband pressure pulse $p_A(t)$ consists of different frequency components $P_\omega(t)$,

$$p_A(t) = \sum_{\omega} P_{0\omega} e^{i\omega t}. \tag{14}$$

Each frequency component is assumed to travel independent of each other

$$\begin{aligned} P_\omega(x,t) &= P_{0\omega} e^{i\omega(t-x/c)} e^{-[\alpha(\omega)/2]x}, \\ I_\omega(x) &= |P_\omega(x,t)|^2 = I_{0\omega} e^{-\alpha(\omega)x}, \end{aligned} \tag{15}$$

where $I_{0\omega} = |P_{0\omega}|^2$ is the initial intensity of that frequency component. Linearity is crucial for guaranteeing lack of interactions and thereby absence of energy transfer between different frequencies ω's. Note that Eq. (15) indicates that $\alpha(\omega)$ is independent of the excitation intensity $I_{0\omega}$ in contrast to the observation here. Any possible energy transfer is not accounted for in the theoretical formulation of attenuation. Therefore nonlinear energy transfer would render the computation of $\alpha(\omega)$ invalid. We will investigate the nonlinear energy transfer to validate the analysis underlying the computation of attenuation cross section.

E. Measurement of encapsulation rheology

The frequency-dependent attenuation due to the microbubble suspension in the acoustic path d is computed using FFTs of the received signal without microbubbles (intensity I^W_ω) and that with them (I^b_ω),

$$\alpha(\omega) = \frac{1}{d} 10 \log_{10} \left(\frac{I^W_\omega}{I^b_\omega} \right). \tag{16}$$

We then determine the interfacial rheological properties (e.g., γ, κ^s, E^s) according to a particular model (NM, CEM, or MM) by minimizing the error between the measured attenuation and theoretical attenuation Eq. (13), the later being defined in terms of the rheological properties Eqs. (11) and (12). The details are provided in our previous publications (Sarkar *et al.*, 2005; Paul *et al.*, 2010; Paul *et al.*, 2013). Note that here, due to the monodisperse nature of the bubble distribution, the expression for attenuation simplifies to being directly proportional to individual attenuation cross section. The attenuation cross section of a contrast microbubble has a peak value at its resonance frequency. Therefore, while determining the interfacial properties, we impose an additional constraint that the modeled attenuation attains its maximum at the same resonance frequency as the experimentally measured one.

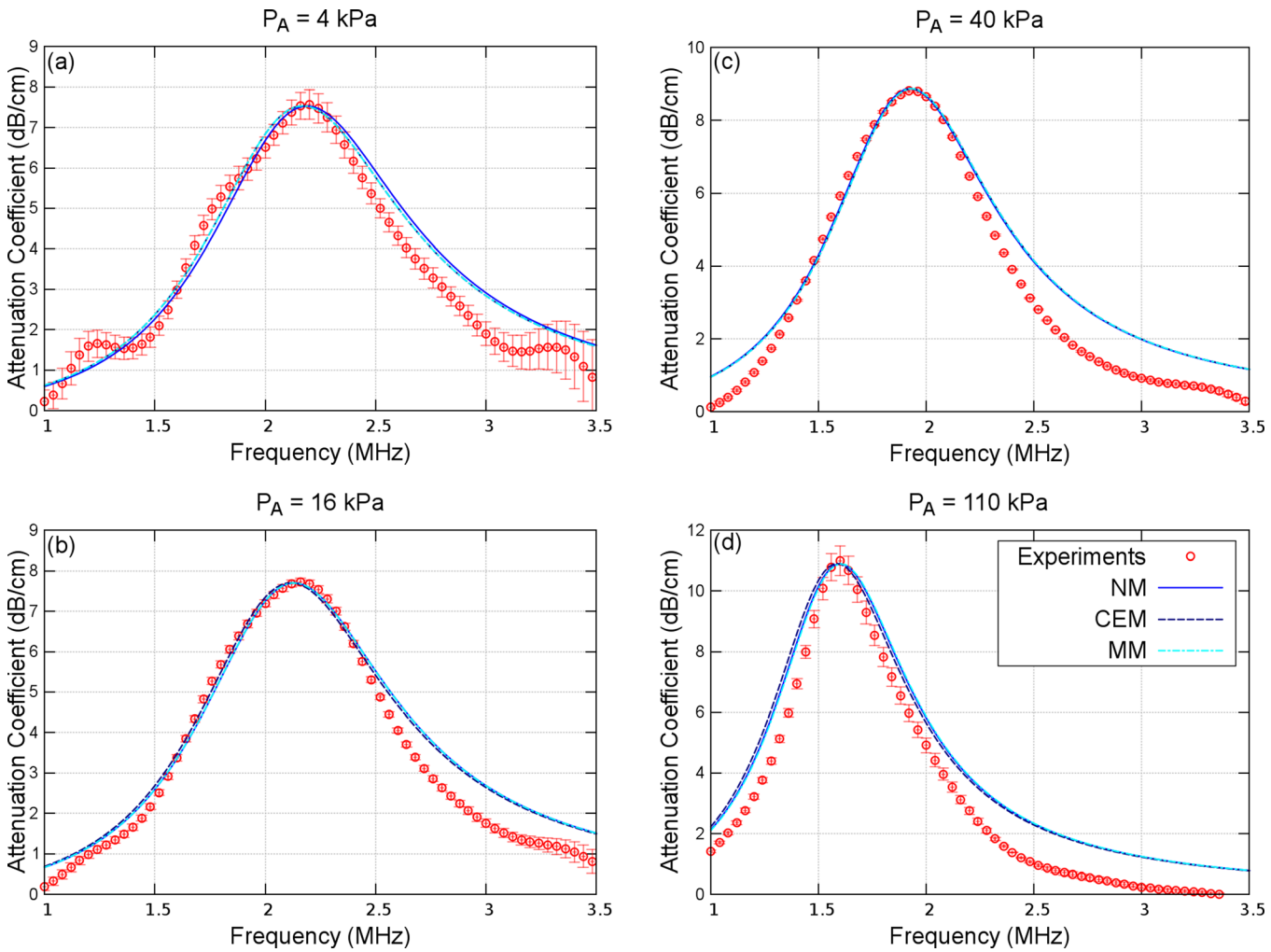

FIG. 3. (Color online) Attenuation curves at 4 different pressure amplitudes (a) 4 kPa, (b) 16 kPa, (c) 40 kPa, and (d) 110 kPa along with the prediction due to CEM model. Predictions due to other models give almost identical curves.

III. RESULTS AND DISCUSSION

A. Pressure-dependent encapsulation rheology

Figures 3(a)–3(d) plot the attenuation spectra for four different acoustic amplitudes—4, 16, 40, and 110 kPa. Note that the peak attenuation value signifying bubble resonance shifts toward lower frequencies—2.19, 2.16, 1.94, and 1.60 MHz—a phenomenon also seen in GCP (Gong *et al.*, 2014). There the resonance frequency—a single value from the attenuation measurement—was used to experimentally obtain the shell elasticity χ according to MM as a function of acoustic pressure amplitude. However, single piece of information (resonance frequency) from each experiment (described by single algebraic equation) is inadequate to simultaneously obtain multiple rheological parameters such as surface dilatational elasticity and surface dilatational viscosity. In fact, in that article the value of dilatational viscosity was assumed known from the literature. Here, we use the entire attenuation data as a function of frequency to obtain the rheological parameters according to three different models—NM, CEM, and MM. We also plot the model predictions in Fig. 3. We note that for this monodisperse microbubbles, all models considered here result in almost identical predictions, unlike what we observed previously for polydisperse contrast microbubbles (Sarkar *et al.*, 2005; Paul *et al.*, 2010).

The rheological parameters for the different models are shown in the Table I. The estimated surface dilatational viscosity value is the same for all models. CEM and MM predict slightly different values for surface dilatational elasticity. Note that for NM, in the absence of dilatational elasticity in the model, the surface tension parameter γ assumes the role of elasticity achieving a very large value (Chatterjee and Sarkar, 2003; Sarkar *et al.*, 2005). In Fig. 4(a) we plot surface tension γ for NM, surface dilatational elasticity E^s for CEM and shell parameter χ (which is identical in nature to E^s) for MM. They all attain very similar values, and show decreasing trend with increasing acoustic pressure amplitude. We also include the values obtained in GCP noting that they follow the same trend. Figure 4(b) shows similar decreasing trend for surface dilatational viscosity with increasing pressure.

TABLE I. Estimated rheological properties of the monodisperse DSPC encapsulated microbubbles corresponding to four different rheological models and four different excitations. It also plots resonance frequency from the experimental data and damping constants according to CEM.

Encapsulation model		Estimated parameters			
	Excitation amplitude	4 kPa	16 kPa	40 kPa	110 kPa
NM	κ^s ($\times 10^{-8}$ N s/m)	2.40 ± 0.03	2.34 ± 0.03	1.97 ± 0.03	1.52 ± 0.05
	γ (N/m)	0.56 ± 0.02	0.52 ± 0.02	0.39 ± 0.02	0.21 ± 0.02
CEM	κ^s ($\times 10^{-8}$ N s/m)	2.40 ± 0.03	2.34 ± 0.03	1.97 ± 0.03	1.52 ± 0.05
	γ_0 (N/m)	0.04 ± 0.01	0.04 ± 0.01	0.04 ± 0.01	0.04 ± 0.01
	E^s (N/m)	0.56 ± 0.04	0.52 ± 0.04	0.39 ± 0.04	0.18 ± 0.04
MM	κ^s ($\times 10^{-8}$ N s/m)	2.40 ± 0.03	2.34 ± 0.03	1.97 ± 0.03	1.52 ± 0.05
	γ (R_0)(N/m)	0.04 ± 0.02	0.04 ± 0.02	0.04 ± 0.02	0.04 ± 0.02
	χ (N/m)	0.56 ± 0.03	0.53 ± 0.03	0.39 ± 0.03	0.19 ± 0.03
f_0 (MHz)		2.19	2.16	1.94	1.60
Damping constant		0.50 ± 0.01	0.50 ± 0.01	0.49 ± 0.01	0.48 ± 0.01
β_{rms} (CEM)		0.0083	0.0297	0.0772	0.1694

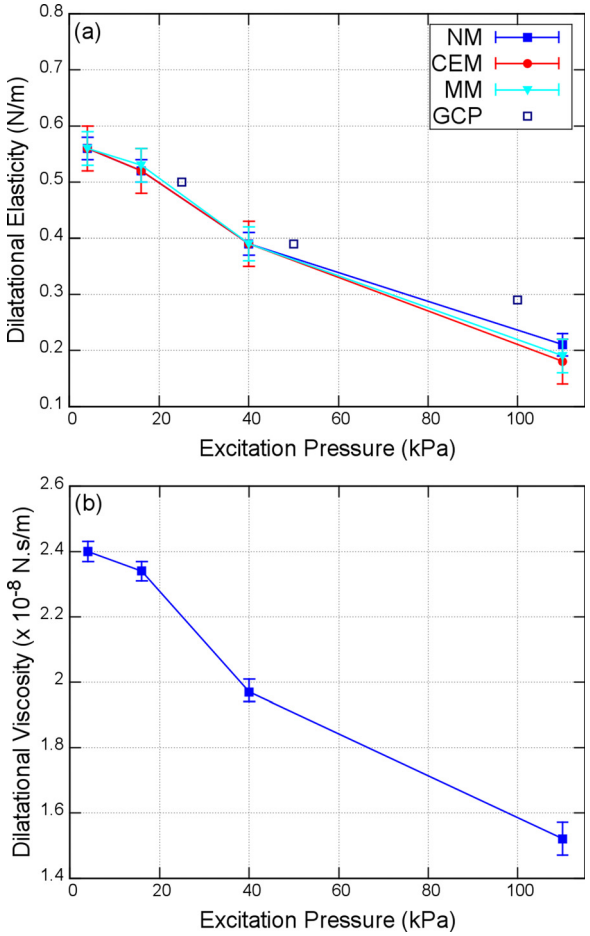

FIG. 4. (Color online) (a) Interfacial dilatational elasticity (surface tension for NM model) and (b) interfacial dilatational viscosity as functions of excitation pressure.

In Table I, we also list the resonance frequency (peak values) from Figs. 3(a)–3(d), as well as the damping constant according to the models. Note that all models result in identical interfacial viscosity for the lipid shell and therefore identical values for δ. In Figs. 5(a) and 5(b), we plot the experimentally measured resonance frequency and the model predicted damping constant, respectively. The resonance frequency decreases but the damping constant remains relatively constant with a mean value of $\delta = 0.49 \pm 0.01$. This can be explained by noting that the damping in Eq. (12) is dominated by the encapsulation damping $\delta_{encapsulation}$. It remains constant as the surface dilatational viscosity κ^s [Fig. 3(b)] and the resonance frequency $\omega_0 = 2\pi f_0$ [Fig. 4(a)] both decrease with the pressure amplitude in the same ratio; κ^s decreases by 36.67% while f_0 decreases by 36.87% over the pressure change from 4 to 110 kPa.

B. Validity of acoustic attenuation analysis: Linear propagation

We use excitation-dependent attenuation to estimate the encapsulation rheology. However, excitation-dependent attenuation plotted in Fig. 3 raises a concern about the

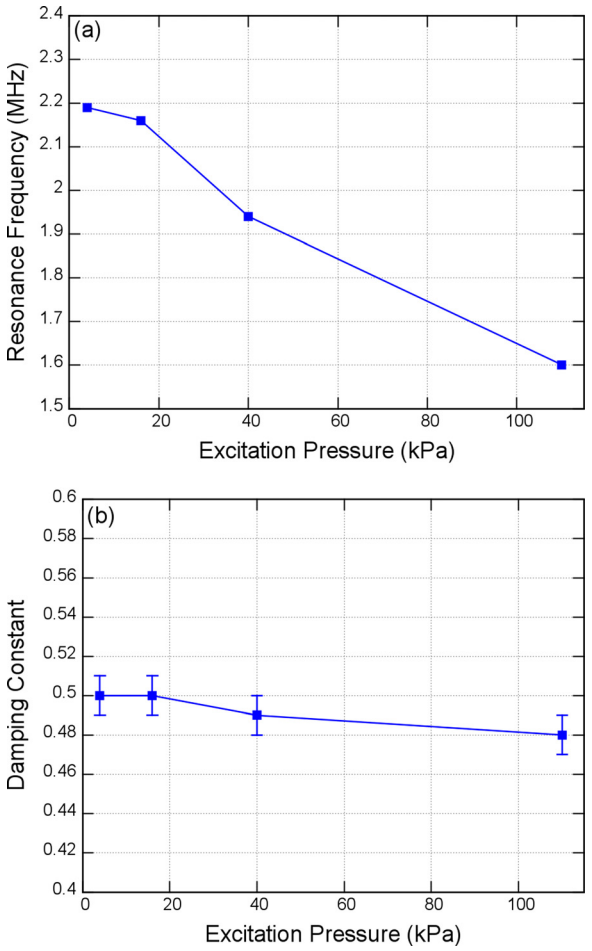

FIG. 5. (Color online) (a) Resonance frequency and (b) damping constant as functions of pressure amplitude.

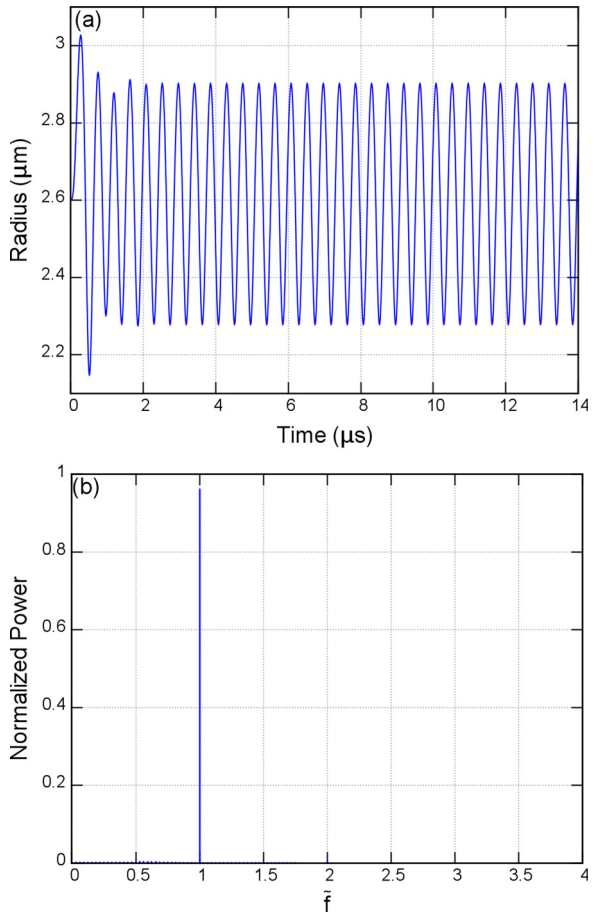

FIG. 6. (Color online) Radial dynamics (a) at 110 kPa pressure excitation and its FFT (b) using CEM model.

nonlinearity of the bubble dynamics and validity of the analysis underlying the computation of attenuation. As noted above, the analysis assumes independence of different frequency components in the propagating pulse and no nonlinear energy transfer between different frequencies. In case of energy transfer between frequencies, it will be hard to differentiate attenuation of individual frequency components during propagation from energy transfer from (toward) the same frequency toward (from) others.

Here, we numerically investigate the extent of nonlinear energy transfer during the propagation of an acoustic wave through a suspension of microbubbles. Note that if we assume that propagation in water is linear (acoustic Mach number $M = \Delta p_{\max}/\rho c^2 \sim 10^{-4}$) as is customary, energy transfer between different frequency components, if any, occurs due to the nonlinear bubble dynamics. Furthermore, even a strong nonlinear energy transfer in individual bubble dynamics might not translate into nonlinear propagation, because bubbles are sparsely distributed along the path of an acoustic pulse. Only very large nonlinear energy transfer in the bubble dynamics can result in nonlinear acoustic wave propagation at sufficient bubble concentration discrediting the analysis used to arrive at the frequency-dependent attenuation discussed here. We compute the radial dynamics of the monodisperse lipid-coated microbubble excited by a monochromatic acoustic pulse with the same frequency as the center frequency of the pulse used in the experiment. We use the full Rayleigh-Plesset Eq. (1) along with the properties determined for the CEM model listed in Table I to compute the radius $R(t)$ at the highest pressure amplitude value, 110 kPa, used in the experiment. The radius as a function of time is plotted in Fig. 6(a). It is transferred to the frequency domain [Fig. 6(b)] by FFT obtaining $\tilde{R}[n]$ which is plotted as a function of frequency $\tilde{f}$ normalized by the excitation frequency. Note the single peak at the excitation frequency. Specifically, we investigate the amount of energy at the excitation frequency 2.25 MHz ($\tilde{f} = 1$), which is indicated as $E[i]$ to find that

$$\frac{E[i]}{E} = \frac{|\tilde{R}[i]|^2}{\sum_{n=1}^{N} |\tilde{R}[n-1]|^2 - \left|\frac{1}{N}\sum_{n=1}^{N} \tilde{R}[n-1]\right|^2} = 0.9580. \tag{17}$$

Note that the dc component of the energy has been subtracted away from the total energy. The corresponding value for MM is very similar $E[i]/E = 0.9638$. The energy in the fundamental frequency being close to the total energy indicates that there is negligible energy transfer between different frequencies even in the radial dynamics. Therefore, acoustic propagation through a medium sparsely populated by these microbubbles is approximately linear rendering the computation of frequency-dependent attenuation valid.

Note that unlike free microbubbles, encapsulated contrast microbubbles have been reported to occasionally show nonlinear behaviors even at low excitations. A very low subharmonic threshold was experimentally observed by some (Shankar *et al.*, 1998, 1999), but not by others (Bhagavatheeshwaran *et al.*, 2004; Sarkar *et al.*, 2005; Kimmel *et al.*, 2007). Using ultra-high frame rate optical observations of individual bubble dynamics Overvelde *et al.* (2010) have uncovered strong nonlinear oscillations with pronounced skewness in the resonance curve for lipid-coated BR14 contrast agent at acoustic excitations as low as 10 kPa. The authors argued that the nonlinear radial dynamics of the individual bubble results from buckling of the encapsulating shell [presumably with nonspherical surface oscillation (Liu *et al.*, 2012)]. They were able to match the observation by simulated radial dynamics using MM with a relatively large value of $\chi = 2.5$ N/m and a small value of $\kappa^s = 6 \times 10^{-9}$ N s/m ($\gamma_0 = 0.02$ N/m). Because of the similarity between BR14 and the lipid-coated microbubbles studied here (note though that the preparation protocols are different), we investigate this model with the values quoted in the paper. However, attenuation computed using these values in MM model is completely different from the measured data (Fig. 7). (Note that there is only one attenuation curve for the one set of parameter values.) Also note that an acoustic investigation of a single BR14 bubble by the same group from University of Twente did not see subharmonic response at 100 kPa excitation (Sijl *et al.*, 2008); there they used different property values to model the observed single bubble behavior—$\chi = 0.54$ N/m and $\kappa^s = 2 \times 10^{-8}$ N s/m. These are the values obtained for BR14 through a different optical experiments by the same group (van der Meer *et al.*, 2007), and are similar to those obtained here. Therefore, supposedly identically prepared encapsulated microbubbles, e.g., BR14, give rise to very different behaviors, sometimes highly nonlinear response for individual microbubble, and linear other times. As we noted before, attenuation is a cumulative phenomenon along the acoustic path passing through many bubbles. It is possible that acoustic wave propagation through a sufficiently concentrated suspension of microbubbles that are experiencing highly nonlinear oscillations, would become nonlinear. Then the analytical theory of attenuation would become invalid.

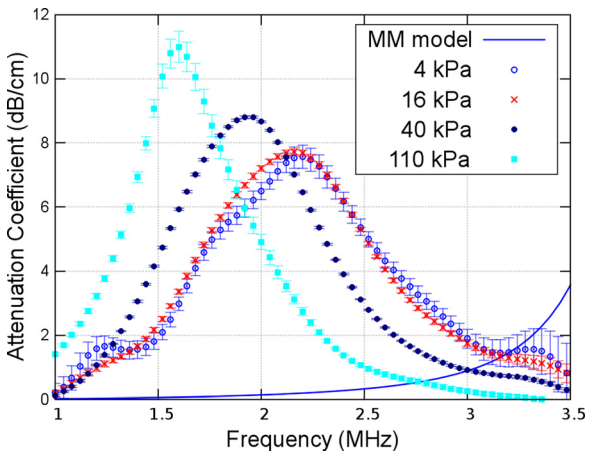

FIG. 7. (Color online) Attenuation measured as a function of frequency at different excitation pressures. The solid line is the attenuation predicted by MM with $\kappa^s = 6 \times 10^{-9}$ N s/m, $\chi = 2.5$ N/m, $\gamma_0 = 0.02$ N/m.

C. Strain-dependent encapsulation rheology: Strain softening

Using attenuation at different amplitude of the pressure pulses, we have found shell properties, i.e., E^s and κ^s, that depend on the pressure pulse amplitude. However, pressure pulse amplitude is not a proper constitutive variable for encapsulation rheology, i.e., rheology cannot be described as a function of pressure amplitude. Instead, based on the principles of continuum mechanics, E^s and κ^s should be functions of the strain and/or the strain rate. The pressure-dependent encapsulation rheology determined here signifies a dependence of the rheological properties on strain. A higher pressure amplitude induces a larger radial oscillation of microbubbles leading to a larger interfacial strain—more specifically larger *"average"* interfacial strain, for in an oscillating microbubble surface strain oscillates between positive and negative maxima. Here, we relate the pressure-dependent rheological properties to such "average strain"-dependent properties.

Note that EEM described in Eq. (6) models strain (areal strain β)-dependent material properties; it is a strain-softening constitutive equation, where strain was computed with reference to the stress-free configuration characterized by R_E. However, this stress-free state varies with E_s and γ, and therefore is different for different pressure amplitude. The EEM cannot be directly used here. Instead, we use a modified EEM model to describe the rheological behavior as a function "nominal average strain"-dependent shell properties:

$$\left.\begin{aligned} E^s &= E_0^s \exp(-\alpha_E^s \beta_{\rm rms}) \\ \kappa^s &= \kappa_0^s \exp(-\alpha_\kappa^s \beta_{\rm rms}) \end{aligned}\right\}$$
$$\beta_{\rm rms} = \left\{ \frac{1}{T} \int_o^T \left(\frac{R^2(t)}{R_0^2} - 1 \right)^2 dt \right\}^{1/2}. \qquad (18)$$

The strain is computed relative to the initial configuration R_0. We use the Rayleigh-Plesset Eq. (1) with the properties determined for the CEM model listed in Table I to numerically simulate the microbubble dynamics and compute $\beta_{\rm rms}$ for each pressure amplitude, listed in Table I. We then fit the relations (18) to obtain the values of E_0^s, κ_0^s, α_E^s, and α_κ^s shown in Table II. The fitted curves are shown in Figs. 8(a) and 8(b).

IV. SUMMARY

A critical investigation of the attenuation of ultrasound through a suspension of monodisperse lipid-coated microbubbles is examined. Specifically, its validity when different values are nominally computed using the data obtained at

TABLE II. The parameters describing the phenomenological relation describing the strain-dependent interfacial elasticity and viscosity according to Eq. (18).

E_0^s (N/m)	α_E^s	κ_0^s ($\times 10^{-8}$ N s/m)	α_κ^s
0.61 ± 0.1	6.55 ± 3.00	2.49 ± 0.15	2.93 ± 1.00

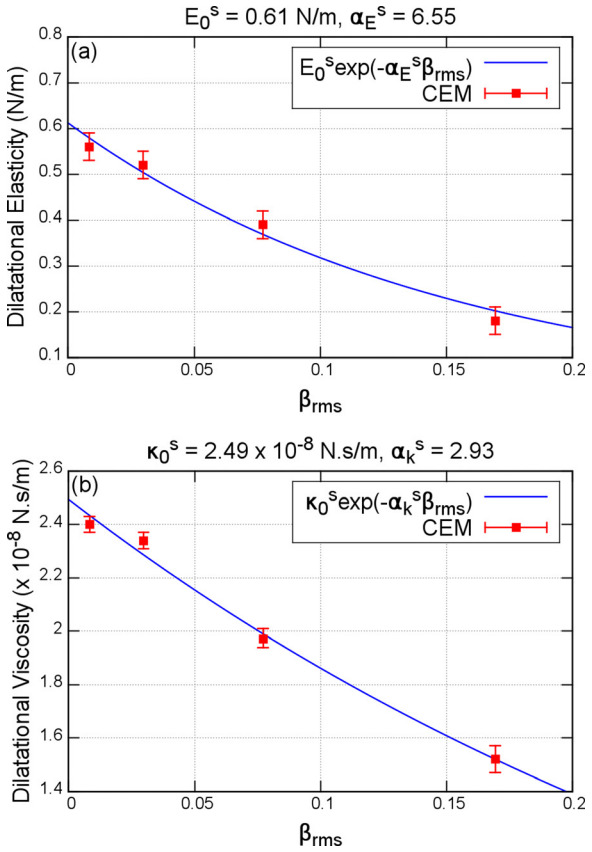

FIG. 8. (Color online) Phenomenological relations for strain-dependent (a) interfacial dilatational elasticity and (b) interfacial dilatational viscosity.

different excitation pressures. The theory of attenuation presupposes linear wave propagation which results in attenuation being independent of excitation. Here, attenuation measured at different pressures shows a downshift in peak with increasing pressure signaling a change in characteristics of the coating. Applying three different interfacial rheology models to the data we determine very similar values of interfacial dilatational elasticity and viscosity for the lipid coating as functions of pressure amplitude. We investigate the bubble dynamics at the excitations used in measurement and find the nonlinearity to be negligible establishing the validity of the attenuation analysis. We relate the pressure-dependent properties to strain-dependent properties showing that the interfacial dilatational viscosity and elasticity decrease with average areal strain. We provide a phenomenological relation for the strain dependence.

We conclude that even though one obtains different attenuation at different excitation pressures, the bubble dynamics as well as acoustic wave propagation through the suspension of the microbubbles remains linear, and therefore the attenuation obtained at different excitation pressures are valid. They indicate not a nonlinear propagation but a constitutive nonlinearity—nonlinear variation in the material properties of the encapsulating shell with increasing strain experienced at increasing pressures. We do note that individual lipid-coated microbubbles have previously shown strongly nonlinear dynamics. However, the same microbubbles, i.e., prepared identically, in other experiments did not, indicating a strong variability in individual bubble behaviors. If a majority of microbubbles in a dense suspension experience nonlinear oscillations, propagation can become nonlinear.

ACKNOWLEDGMENTS

This work is partially supported by NSF Grant Nos. CBET-1205322 and DMR-1239105.

Ainslie, M. A., and Leighton, T. G. (**2011**). "Review of scattering and extinction cross-sections, damping factors, and resonance frequencies of a spherical gas bubble," J. Acoust. Soc. Am. **130**, 3184–3208.

Bhagavatheeshwaran, G., Shi, W. T., Forsberg, F., and Shankar, P. M. (**2004**). "Subharmonic signal generation from contrast agents in simulated neovessels," Ultrasound Med. Biol. **30**, 199–203.

Chatterjee, D., Jain, P., and Sarkar, K. (**2005a**). "Ultrasound-mediated destruction of contrast microbubbles used for medical imaging and drug delivery," Phys. Fluids **17**, 100603.

Chatterjee, D., and Sarkar, K. (**2003**). "A Newtonian rheological model for the interface of microbubble contrast agents," Ultrasound Med. Biol. **29**, 1749–1757.

Chatterjee, D., Sarkar, K., Jain, P., and Schreppler, N. E. (**2005b**). "On the suitability of broadband attenuation measurement for characterizing contrast microbubbles," Ultrasound Med. Biol. **31**, 781–786.

Church, C. C. (**1995**). "The effects of an elastic solid-surface layer on the radial pulsations of gas-bubbles," J. Acoust. Soc. Am. **97**, 1510–1521.

deJong, N. (**1996**). "Improvements in ultrasound contrast agents," IEEE Eng. Med. Biol. Mag. **15**, 72–82.

deJong, N., Hoff, L., Skotland, T., and Bom, N. (**1992**). "Absorption and scatter of encapsulated gas filled microspheres—Theoretical considerations and some measurements," Ultrasonics **30**, 95–103.

deJong, N., Tencate, F. J., Lancee, C. T., Roelandt, J. R. T. C., and Bom, N. (**1991**). "Principles and recent developments in ultrasound contrast agents," Ultrasonics **29**, 324–330.

Doinikov, A. A., and Dayton, P. A. (**2007**). "Maxwell rheological model for lipid-shelled ultrasound microbubble contrast agents," J. Acoust. Soc. Am. **121**, 3331–3340.

Goldberg, B. B., Raichlen, J. S., and Forsberg, F. (**2001**). *Ultrasound Contrast Agents: Basic Principles and Clinical Applications* (Martin Dunitz, London), p. 440.

Gong, Y., Cabodi, M., and Porter, T. (**2010**). "Relationship between size and frequency dependent attenuation of monodisperse populations of lipid coated microbubbles," Bubble Sci., Eng., Technol. **2**, 41–47.

Gong, Y. J., Cabodi, M., and Porter, T. M. (**2014**). "Acoustic investigation of pressure-dependent resonance and shell elasticity of lipid-coated monodisperse microbubbles," Appl. Phys. Lett. **104**, 074103.

Hoff, L., Sontum, P. C., and Hovem, J. M. (**2000**). "Oscillations of polymeric microbubbles: Effect of the encapsulating shell," J. Acoust. Soc. Am. **107**, 2272–2280.

Katiyar, A., and Sarkar, K. (**2010**). "Stability analysis of an encapsulated microbubble against gas diffusion," J. Colloid Interface Sci. **343**, 42–47.

Katiyar, A., and Sarkar, K. (**2011**). "Excitation threshold for subharmonic generation from contrast microbubbles," J. Acoust. Soc. Am. **130**, 3137–3147.

Katiyar, A., and Sarkar, K. (**2012**). "Effects of encapsulation damping on the excitation threshold for subharmonic generation from contrast microbubbles," J. Acoust. Soc. Am. **132**, 3576–3585.

Katiyar, A., Sarkar, K., and Jain, P. (**2009**). "Effects of encapsulation elasticity on the stability of an encapsulated microbubble," J. Colloid Interface Sci. **336**, 519–525.

Kimmel, E., Krasovitski, B., Hoogi, A., Razansky, D., and Adam, D. (**2007**). "Subharmonic response of encapsulated microbubbles: Conditions for existence and amplification," Ultrasound Med. Biol. **33**, 1767–1776.

Liu, Y. Q., Sugiyama, K., Takagi, S., and Matsumoto, Y. (**2012**). "Surface instability of an encapsulated bubble induced by an ultrasonic pressure wave," J. Fluid Mech. **691**, 315–340.

Marmottant, P., van der Meer, S., Emmer, M., Versluis, M., de Jong, N., Hilgenfeldt, S., and Lohse, D. (**2005**). "A model for large amplitude oscillations of coated bubbles accounting for buckling and rupture," J. Acoust. Soc. Am. **118**, 3499–3505.

Medwin, H. (**1977**). "Counting bubbles acoustically—Review," Ultrasonics **15**, 7–13.

Morgan, K. E., Allen, J. S., Dayton, P. A., Chomas, J. E., Klibanov, A. L., and Ferrara, K. W. (**2000**). "Experimental and theoretical evaluation of microbubble behavior: Effect of transmitted phase and bubble size," IEEE Trans. Ultrason. Ferroelectr. Freq. Control **47**, 1494–1509.

Overvelde, M., Garbin, V., Sijl, J., Dollet, B., de Jong, N., Lohse, D., and Versluis, M. (**2010**). "Nonlinear shell behavior of phospholipid-coated microbubbles," Ultrasound Med. Biol. **36**, 2080–2092.

Patel, D., Dayton, P., Gut, J., Wisner, E., and Ferrara, K. W. (**2002**). "Optical and acoustical interrogation of submicron contrast agents," IEEE Trans. Ultrason. Ferroelectr. Freq. Control **49**, 1641–1651.

Paul, S., Katiyar, A., Sarkar, K., Chatterjee, D., Shi, W. T., and Forsberg, F. (**2010**). "Material characterization of the encapsulation of an ultrasound contrast microbubble and its subharmonic response: Strain-softening interfacial elasticity model," J. Acoust. Soc. Am. **127**, 3846–3857.

Paul, S., Russakow, D., Nahire, R., Nandy, T., Ambre, A. H., Katti, K., Mallik, S., and Sarkar, K. (**2012**). "*In vitro* measurement of attenuation and nonlinear scattering from echogenic liposomes," Ultrasonics **52**, 962–969.

Paul, S., Russakow, D., Rodgers, T., Sarkar, K., Cochran, M., and Wheatley, M. A. (**2013**). "Determination of the interfacial rheological properties of a Poly(DL-lactic acid)-encapsulated contrast agent using *in vitro* attenuation and scattering," Ultrasound Med. Biol. **39**, 1277–1291.

Sarkar, K., Katiyar, A., and Jain, P. (**2009**). "Growth and dissolution of an encapsulated contrast microbubble," Ultrasound Med. Biol. **35**, 1385–1396.

Sarkar, K., and Prosperetti, A. (**1994**). "Coherent and incoherent-scattering by oceanic bubbles," J. Acoust. Soc. Am. **96**, 332–341.

Sarkar, K., Shi, W. T., Chatterjee, D., and Forsberg, F. (**2005**). "Characterization of ultrasound contrast microbubbles using *in vitro* experiments and viscous and viscoelastic interface models for encapsulation," J. Acoust. Soc. Am. **118**, 539–550.

Shankar, P. M., Krishna, P. D., and Newhouse, V. L. (**1998**). "Advantages of subharmonic over second harmonic backscatter for contrast-to-tissue echo enhancement," Ultrasound Med. Biol. **24**, 395–399.

Shankar, P. M., Krishna, P. D., and Newhouse, V. L. (**1999**). "Subharmonic backscattering from ultrasound contrast agents," J. Acoust. Soc. Am. **106**, 2104–2110.

Sijl, J., Gaud, E., Frinking, P. J. A., Arditi, M., de Jong, N., Lohse, D., and Versluis, M. (**2008**). "Acoustic characterization of single ultrasound contrast agent microbubbles," J. Acoust. Soc. Am. **124**, 4091–4097.

van der Meer, S. M., Dollet, B., Voormolen, M. M., Chin, C. T., Bouakaz, A., de Jong, N., Versluis, M., and Lohse, D. (**2007**). "Microbubble spectroscopy of ultrasound contrast agents," J. Acoust. Soc. Am. **121**, 648–656.